

Angular dependent magnetization reversal in exchange biased bilayers under a modified ‘effective field model’

Wei Zhang, Qing-feng Zhan, and Kannan M. Krishnan *

*Department of Materials Science, University of Washington, Seattle, Washington
98195, USA*

Abstract

A modified effective field model was developed to quantitatively interpret the angular dependent magnetization reversal processes in exchange biased Fe/IrMn bilayers. Several kinds of multi-step loops with distinct magnetization reversal routes were observed for the samples measured at various field orientations. Two types of angular dependent switching fields are observed and their transitions are investigated, which are found to be driven by both Fe and IrMn layer thicknesses. Our modified effective field model can nicely describe all the switching field behaviors including the critical effects of the exchange bias induced uniaxial anisotropy on the magnetization reversal processes.

PACS numbers: 75.70.Cn, 75.60.Jk, 75.30.Gw

* Author to whom correspondence should be addressed. Email: kannanmk@uw.edu

I. Introduction

Exchange bias (EB) of ferromagnetic (F) / antiferromagnetic (AF) bilayers has been extensively studied in the past decades due to its key role in magnetic recording technologies¹. One of the intriguing properties of EB is the asymmetric magnetization reversal behavior², however, whose origin still remains controversial. Such asymmetric behavior has been correlated, depending on the nature of the bilayers, with different magnetization processes²⁻⁷, and the angle between the external field and the EB direction⁸⁻¹⁰. To probe such properties, the angular dependent magnetic measurement has been widely adopted with various experimental setups such as the vector magneto-optic Kerr effect (MOKE)^{11,12}, which offers a comprehensive understanding of the magnetic reversal processes by probing both the longitudinal and transverse magnetization components.

The magnetic reversal processes in magnetic films are determined by the magnetic anisotropies¹³. In polycrystalline EB bilayers, a unidirectional anisotropy, K_{eb} , established by EB as well as an induced uniaxial anisotropy, K_{u} , are introduced, which play the key role on altering the magnetic switching process. Considering both K_{eb} and K_{u} , the value of EB, H_{eb} , and coercivity, H_{c} , can be numerically fitted by the Stoner-Wahlfarth model³. In epitaxial EB systems, the intrinsic symmetry of the magnetocrystalline anisotropy needs to be further considered, which results in the multi-step hysteresis loops and a complex angular dependent behavior^{14,15}. An effective field model (EFM), taking into account the unidirectional anisotropy field,

H_X , and the cubic ferromagnetic anisotropy field, H_A , was proposed to quantitatively interpret the complicated angular dependent switching fields¹⁴. Recent studies also showed that both H_A and H_X are inversely proportional to the ferromagnetic layer thickness and are therefore interface related effects¹⁵.

In this work, we systematically studied the magnetization reversal behaviors of Fe/IrMn EB bilayers. By tuning the IrMn layer thickness, t_{IrMn} , the magnetization reversal characteristic in the case of both $H_A > H_X$ and $H_A < H_X$ were obtained. Different types of angular dependent switching fields were observed for each case and were interpreted by the modified effective field model (mEFM) that considers H_X , H_A and an EB induced uniaxial anisotropy H_U . It should be noted that H_U in continuous films can also be induced by various origins including surface steps¹⁶ and oblique growth^{17,18}. By tuning the Fe layer thickness, t_{Fe} , we showed that the different angular dependent behaviors are not a sole function of the anisotropy ratio, H_A/H_X as described in the EFM, but also critically depends on the induced H_U , especially when H_A and H_X are of comparable magnitudes. The induced H_U can give out a new set of angular dependent behaviors in the phase diagram that summarizes all the possible angular dependent magnetization reversal processes. The critical effect of the H_U on the magnetization reversals, which are well described by mEFM, is particularly important in magnetic thin-film devices that require accurate controls on the magnetic switchings.

II. Experiment

Fe/IrMn bilayers were grown on MgO(001) substrates by Ion Beam Sputtering (IBS) with a base pressure below 1×10^{-8} mbar and a deposition rate as low as 1 \AA/s ¹⁹. The substrates were pre-annealed at 500 °C for 1.5 hour and held at 130 °C for the deposition of Fe and IrMn layers. A permanent magnet with a magnetic field ~ 300 Oe was positioned along the Fe[100] direction during growth. Two series of samples (A and B) were grown with the structure of MgO/Fe(t_{Fe})/IrMn(t_{IrMn})/Ta(3nm cap). Series A has a fixed $t_{\text{IrMn}} = 4.5$ nm, and different $t_{\text{Fe}} = 10$ nm (A_{10}), 30 nm (A_{30}), 50 nm (A_{50}), and 70 nm (A_{70}); series B has fixed $t_{\text{IrMn}} = 8$ nm, and different $t_{\text{Fe}} = 10$ nm (B_{10}), 30 nm (B_{30}), 50 nm (B_{50}), and 70 nm (B_{70}). X-ray diffraction (XRD) with Cu $K\alpha$ radiation is used to examine the crystal structure of the samples. The (002) peaks of Fe and IrMn in the longitudinal θ - 2θ scan (Fig. 1(a)) indicated a good out-of-plane (002) texture of the samples²⁰.

III. Results and discussions

Magnetic properties were characterized at room temperature by combined measurements of the longitudinal (\parallel) and transverse (\perp) MOKE for different field orientation, ϕ , which is defined as the angle between the external applied field and the field cooling direction, with ϕ increasing in the clockwise direction. The EB gives rise to the unidirectional anisotropy, H_X , and a collinear uniaxial anisotropy, H_U , along the field cooling direction. Both of them are superimposed on the Fe cubic

magnetocrystalline anisotropy (Fig. 1(b)), thus inducing various magnetic switching routes between the Fe easy axes.

Different magnetic reversal processes as well as the angular dependent behaviors are found in A_{10} and B_{10} . At $|\phi| < 40^\circ$, the magnetic transitions for A_{10} in the descending branch take place at H_{c1} and H_{c2} , with $H_{c1} > H_{c2}$ ($10^\circ < |\phi| < 40^\circ$), Fig. 2(b). The transverse MOKE loop reveals that the first step is an intermediate state in which Fe spins are oriented along the $[010]$ axis for $10^\circ < \phi < 40^\circ$, and along the $[0-10]$ axis for $-40^\circ < \phi < -10^\circ$, when the magnetization switches from the $[100]$ to $[-100]$ directions. The magnetic transition displays a single step at H_{c1} , with $H_{c1} < H_{c2}$, at $|\phi| < 10^\circ$, Fig. 2(a). For the ascending branch, however, the magnetization switches smoothly from $[-100]$ to $[100]$ direction without resting at any intermediate state, suggesting that the magnetization reversal occurs by 180° DW nucleation¹⁵. The magnetization reversal for B_{10} in the descending branch is the same process as A_{10} . However, for the ascending branch, the direct 180° magnetic switching cannot be observed but is replaced by a two-step reversal (Fig. 2(f)), i.e., the magnetic transitions take place at H_{c3} and H_{c4} , with $H_{c3} < H_{c4}$ ($15^\circ < |\phi| < 40^\circ$). It should be noted that H_{c3} and H_{c4} belong to the same semicircle as H_{c1} and H_{c2} , as revealed by the transverse MOKE signals. When $H_{c3} > H_{c4}$ ($|\phi| < 15^\circ$), only a one-step reversal at H_{c3} can be observed (Fig. 2(e)). Detailed discussions about the two successive magnetic transitions can be found elsewhere^{21,22}. For the field applied around the Fe hard axes, i.e., $40^\circ < |\phi| < 50^\circ$, hysteresis loops with only one irreversible transition on both branches are observed for both samples (Fig. 2(c) and (g)). Double-shifted loops

with two-stage magnetic transitions occurring on both branches (H_{c5} , H_{c6} for the descending branch and H_{c7} , H_{c8} for the ascending branch) are observed for both samples at $50^\circ < |\phi| < 130^\circ$, far away from the bias direction (Fig. 2(d) and (h)). The transverse MOKE loops show the intermediate state for the ascending and descending branches lie on the same axis given by the bias, i.e., the [100] direction, and the switching route is [0-10] \rightarrow [100] \rightarrow [010] for decreasing field and the reverse route for increasing field.

The angular dependent switching fields for A₁₀ and B₁₀ are summarized in Figure 3. The data is presented in two different field regions, (1) $\phi_{||}$, for the field orientation $\phi = \phi_0 + \Delta\phi$ with $\phi_0 = 0^\circ$ and $-40^\circ < \Delta\phi < 40^\circ$, i.e., close to the bias direction; (2) ϕ_{\perp} , for the field orientation $\phi = \phi_0 + \Delta\phi$ with $\phi_0 = -90^\circ$ and $-40^\circ < \Delta\phi < 40^\circ$, i.e., close to perpendicular to the bias direction. Here, we use the mEFM to quantitatively interpret the angular dependence of the switching fields. The effective field, H_{eff} , is considered to come from four different contributions rather than three as it was originally proposed, i.e., the external magnetic field, H_{ext} , the exchange field, H_X , the EB induced uniaxial anisotropy field, H_U , and the cubic anisotropy field, H_A , which is aligned with the Fe easy axis. Notably, both H_A and H_U depend on the projection of the ferromagnetic magnetization onto the Fe easy axis.

The switching fields can be derived by comparing the effective fields at the initial and final Fe easy axes involved in the magnetic transition^{14,15}. The theoretical switching fields for 90° magnetic transitions are obtained as:

$$H_{c1} = - (H_X + H_A + H_U) / (\cos \Delta\phi + \sin \Delta\phi),$$

$$H_{c2} = -(H_X + H_A - H_U) / (\cos \Delta \phi - \sin \Delta \phi),$$

$$H_{c3} = -(H_X - H_U - H_A) / (\cos \Delta \phi - \sin \Delta \phi),$$

$$H_{c4} = -(H_X + H_U - H_A) / (\cos \Delta \phi + \sin \Delta \phi),$$

$$H_{c5} = -(H_A - H_U - H_X) / (\cos \Delta \phi - \sin \Delta \phi),$$

$$H_{c6} = -(H_A + H_U + H_X) / (\cos \Delta \phi + \sin \Delta \phi),$$

$$H_{c7} = (H_A - H_U - H_X) / (\cos \Delta \phi + \sin \Delta \phi),$$

$$H_{c8} = (H_A + H_U + H_X) / (\cos \Delta \phi - \sin \Delta \phi).$$

For 180° magnetic switching from the [-100] to [100] axes,

$$H_c = (H_A - H_X + H_U) / \cos \Delta \phi.$$

As can be seen in Fig. 2 and 3, the characterizing switching fields of A_{10} satisfy $H_{c1} < 0$, $H_{c2} < 0$, and $H_c > 0$ within ϕ_{\parallel} . A relationship of the effective fields $H_A > H_X - H_U$ can be therefore predicted according to the above equations. Similarly, we found the switching fields $H_{c1} < 0$, $H_{c2} < 0$, $H_{c3} < 0$, and $H_{c4} < 0$ for B_{10} , indicating $H_X > H_A \pm H_U$. Within ϕ_{\perp} , the switching fields for A_{10} satisfy $H_{c5}, H_{c6} < 0$ and $H_{c7}, H_{c8} > 0$, thus $H_A > H_X + H_U$. However, the switching fields for B_{10} satisfy $H_{c6}, H_{c7} < 0$ and $H_{c5}, H_{c8} > 0$, which indicates $H_X > H_A - H_U$. Here, we label the angular dependent switching fields for A_{10} as type-I₀ (at ϕ_{\parallel}) and type-I₉₀ (at ϕ_{\perp}) behavior (Fig. 2(a-b)), and for B_{10} as type-II₀ (at ϕ_{\parallel}) and type-II₉₀ (at ϕ_{\perp}) behavior (Fig. 2(c-d)). Each type of angular dependent behavior has its distinct characterizing switching fields and effective field relationships (Table 1). Notably, in the original EFM which excludes H_U , the effective field relationships regresses to two simple ones, i.e., $H_A > H_X$ for Type-I_{0,90} and $H_A < H_X$ for Type-II_{0,90}.

Using the above-derived expressions, the angular dependence of the switching fields for A₁₀ and B₁₀ can be well fitted (Fig. 3). Our fitting gave the anisotropy fields: $H_A = 55$ Oe, $H_X = 19$ Oe, $H_U = 6$ Oe for A₁₀; and $H_A = 20$ Oe, $H_X = 45$ Oe, $H_U = 4$ Oe for B₁₀. Using the relation $J_{\text{ex}} = H_X M_{\text{Fe}} t_{\text{Fe}}$ and the magnetization for bulk Fe, $M_{\text{Fe}} = 1700$ emu/cm³, and $t_{\text{Fe}} = 10$ nm, the interface energy, J_{ex} , between Fe and IrMn is obtained as 0.032 erg/cm² for A₁₀ and 0.077 erg/cm² for B₁₀. The fitting results further confirmed that both H_A and H_X are interfacial related effects, which also points directly to the competing effects of the pinned and rotatable AF spins at the F/AF interface²³⁻²⁶. Specifically, for sample A₁₀ with $t_{\text{IrMn}} = 4.5$ nm, the AF anisotropy energy is not strong enough to fully establish the bias. Sufficient numbers of the AF spins at the interface would reverse with the F spins due to the strong exchange coupling, and contribute to the rotatable ferromagnetic anisotropy, H_A , rather than be pinned and enhance H_X . For sample B₁₀, the increased $t_{\text{IrMn}} (= 8\text{ nm})$ results in more AF spins being pinned and less of them being rotatable. Thus an increase in H_X , but a decrease in H_A are observed. This observation is analogous to the competing effect of H_{eb} and H_c in polycrystalline EB bilayers²⁷.

In the original EFM, the Type-I₀ (Type-II₀) angular dependent behavior is predicted to show up simultaneously with Type-I₉₀ (Type-II₉₀) according to the effective field relationships. This has found no problems in the reported Fe/MnF₂¹⁴ and Fe/MnPd EB¹⁵ systems; as in both cases H_A is significantly larger than H_X . Nevertheless, as we have demonstrated in the mEFM, taking into account the H_U discriminates the critical conditions for the type-I₀ and type-I₉₀ angular dependent

behaviors, as well as for type-II₀ and type-II₉₀. By comparing those critical conditions, we predict theoretically that the observation of type-II₀ should simultaneously lead to the observation of type-II₉₀, since $H_X > H_A - H_U \subset H_X > (H_A \pm H_U)$; however, the observation of type-I₀ does not necessarily lead to the observation of type-I₉₀, because $H_A > H_U + H_X \not\subset H_A > H_X - H_U$. In other words, it is possible to observe the combination of both type-I₀ and type-II₉₀ when the relationship $H_U + H_X > H_A > H_X - H_U$ is satisfied. This critical effect of H_U is particularly significant when H_A and H_X are of comparable magnitude.

To investigate the critical effect of H_U , MOKE angular dependent measurements were further performed on all A and B series samples. For the A series, all samples are characterized by the switching fields $H_{c>} > 0$, $H_{c5} < 0$, $H_{c7} > 0$, and display the type-I_{0,90} behavior. mEFM fittings gave out the relationship $H_A > H_X \pm H_U$ for all samples, A₁₀-A₇₀. For the B series samples, fully biased hysteresis loops are observed for B₁₀ and B₃₀ when measuring along the bias direction, but not for B₅₀ and B₇₀. On the other hand, loops measured perpendicular to the bias direction have the same feature of $H_{c5} > 0$, $H_{c6} < 0$, $H_{c7} < 0$ and $H_{c8} > 0$. The angular dependence of switching fields for B₃₀ displays the type-II_{0,90} behavior (Fig. 4(a) and (d)). Compared with B₁₀, the evolution via increasing t_{Fe} can be recognized by the larger onset $|\Delta\phi|$ for H_{c4} , and also the smaller values of $|H_{c4}|$, $|H_{c5}|$ and $|H_{c7}|$. As the Fe layer thickness further increases, the angular dependent behaviors for B₅₀ and B₇₀ changed from the type-II_{0,90} to the combination of type-I₀ (Fig. 4(b) and (c)) and type-II₉₀ (Fig. 4(e) and (f)) behavior, with the 180° magnetic transition taking place in the whole range of $\phi_{||}$ for the

ascending branch. We fitted the curves for each sample and the parameters are summarized in Table 2. Consistently, the anisotropy fields satisfy the relationship of $H_X > H_A + H_U$ for B₁₀ and B₃₀, but $H_U + H_X > H_A > H_X - H_U$ for B₅₀ and B₇₀, respectively. As can be seen, the induced H_U , though quite small, can also significantly alter the magnetization reversal processes. A phase diagram shows the different sets of angular dependent behavior is varied with the ratio $(H_X - H_U)/H_A$ and $(H_X + H_U)/H_A$, as plotted in Fig. 5. In the original EFM, only two sets of angular dependence, i.e., type-I_{0,90} and type-II_{0,90}, are predicted to appear on either side of the critical point of $H_X = H_A$. The induced H_U in our mEFM results in the new set of combination (type-I₀, type-II₉₀) where $H_U + H_X > H_A > H_X - H_U$ is satisfied.

IV. Conclusion

In summary, the magnetic properties of Fe/IrMn EB bilayers with different Fe and IrMn thicknesses were characterized using vector MOKE. Square loops, asymmetric-shaped loops, and different two-step loops were observed when measuring at various field orientations. Two sets of typical angular dependent switching fields and their transitions are investigated, which are found to be driven by both Fe and IrMn layer thicknesses. Considering the cubic, the uniaxial, and the unidirectional anisotropies, we developed a mEFM that nicely describes the different magnetization reversal processes together with the two types of angular dependent behaviors. The induced uniaxial anisotropy can significantly alter the critical onsets

for the different angular dependent switching fields, as demonstrated both experimentally and theoretically. A phase diagram describing the angular dependent behaviors with the relative magnitudes of the effective fields was also plotted.

ACKNOWLEDGEMENT

This work was supported by DoE/BES under Grant No. ER45987.

References:

- [1] W. H. Meilkejohn, C. P. Bean, Phys. Rev **102** 1413 (1956)
- [2] M. Fitzsimmons, P. Yashar, C. Leighton, I. K. Schuller, J. Nogues, C. Majkrzak, and J. Dura, Phys. Rev. Lett. **84** 3986 (2000)
- [3] J. Camarero, J. Sort, A. Hoffmann, J. M. Garcia-Martin, B. Dieny, R. Miranda, and J. Nogues, Phys. Rev. Lett. **96** 217205 (2006)
- [4] Z. -P. Li, O. Petravic, R. Morales, J. Olamit, X. Batlle, K. Liu, and I. K. Schuller, Phys. Rev. Lett. **96** 217205 (2006)
- [5] C. Leighton, M. Fitzsimmons, P. Yashar, A. Hoffmann, J. Nogues, J. Dura, C. Majkrzak, and I. K. Schuller, Phys. Rev. Lett. **86** 4394 (2001)
- [6] P. Blomqvist, K. M. Krishnan, and H. Ohldag, Phys. Rev. Lett. **94** 107203 (2005)
- [7] F. Radu, M. Etzkorn, R. Siebrecht, T. Schmitte, K. Westerholt, and H. Zabel, Phys. Rev. B **67** 134409 (2003)
- [8] A. Tillmanns, S. Oertker, B. Beschoten, G. Guntherodt, J. Eisenmenger, and I. K.

- Schuller, Phys. Rev. B. **78** 012401 (2008)
- [9] T. Tillmanns, S. Oertker, B. Beschoten, G. Guntherodt, C. Leighton, I. K. Schuller, and J. Nogues, Appl. Phys. Lett. **89** 202512 (2006)
- [10] P. Y. Yang, C. Song, B. Fan, F. Zeng, and F. Pan, J. Appl. Phys. **106** 013902 (2009)
- [11] J. M. Florczak, and E. D. Dahlberg, J. Appl. Phys. **67** 7520 (1990)
- [12] H. Ohldag, N. B. Weber, F. U. Hillebrecht, and E. Kisker, J. Appl. Phys. **91** 2228 (2002)
- [13] M. T. Johnson, P. J. H. Bloemen, F. J. A. den Broeder, and J. J. de Vries, Rep. Prog. Phys. **59** 1409 (1996)
- [14] E. Arenholz, and K. Liu, Appl. Phys. Lett. **87** 132501 (2005)
- [15] Q. Zhan, and K. M. Krishnan, J. Appl. Phys. **107** 09D703 (2010)
- [16] J. Chen, and J. L. Erskine, Phys. Rev. Lett. **68** 1212 (1992)
- [17] Q. Zhan, C. V. Haesendonck, S. Vandezande, and K. Temst, Appl. Phys. Lett. **94** 042504 (2009)
- [18] W. Zhang, D. N. Weiss, and K. M. Krishnan, J. Appl. Phys. **107** 09D724 (2010)
- [19] N. Cheng, J. P. Ahn, and K. M. Krishnan, J. Appl. Phys. **89** 6597 (2001)
- [20] S. G. Wang, A. Kohn, C. Wang, A. K. Petford-Long, S. Lee, R. Fan, J. P. Goff, L. J. Singh, Z. H. Barber, and R. C. C. Ward, J. Phys. D: Appl. Phys. **42** 225001 (2009)
- [21] Q. F. Zhan, S. Vandezande, K. Temst, and C. V. Haesendonck, New. J. Phys. **11** 063003 (2009)
- [22] Q. F. Zhan, S. Vandezande, K. Temst, and C. V. Haesendonck, Phys. Rev. B **80**

094416 (2009)

[23] F. Radu, A. Westphalen, K. Theis-Brohl, and H. Zabel, J. Phys.: Condens. Matter.

18 L29 (2006)

[24] S. K. Mishra, F. Radu, S. Valencia, D. Schmitz, E. Schierle, H. A. Durr, and W.

Eberhardt, Phys. Rev. B **81** 212404 (2010)

[25] S. Bruck, G. Schutz, E. Goering, X. Ji, and K. M. Krishnan, Phys. Rev. Lett. **101**

126402 (2008)

[26] J. Wu, J. S. Park, W. Kim, E. Arenholz, M. Liberati, A. Scholl, Y. Z. Wu, C.

Hwang, and Z. Q. Qiu, Phys. Rev. Lett. **104** 217204 (2010)

[27] D. Spenato, V. Castel, S. P. Pogossian, D. T. Dekadjevi, and J. B. Youssef, Appl.

Phys. Lett. **91** 062515 (2007)

TABLE and FIGURE CAPTIONS:

| range | Type | Characterizing switching fields | Effective fields relationship (mEFM) | Effective fields relationship (EFM) |
|----------------|-----------------------|--|--------------------------------------|-------------------------------------|
| $\phi_{ }$ | Type-I ₀ | $H_{c1}, H_{c2} < 0, H_c > 0$ | $H_A > H_X - H_U$ | $H_A > H_X$ |
| | Type-II ₀ | $H_{c1}, H_{c2}, H_{c3}, H_{c4} < 0$ | $H_X > H_A \pm H_U$ | $H_X > H_A$ |
| ϕ_{\perp} | Type-I ₉₀ | $H_{c5}, H_{c6} < 0, H_{c7}, H_{c8} > 0$ | $H_A > H_X + H_U$ | $H_A > H_X$ |
| | Type-II ₉₀ | $H_{c6}, H_{c7} < 0, H_{c5}, H_{c8} > 0$ | $H_X > H_A - H_U$ | $H_X > H_A$ |

Table. 1 Summary of the characterizing switching fields and the effective fields relationship of the different types of angular dependent behaviors for mEFM and EFM.

| Sample | H_A / Oe | H_X / Oe | H_U / Oe |
|-----------------|------------|------------|------------|
| B ₁₀ | 20 | 45 | 4 |
| B ₃₀ | 9 | 18 | 3 |
| B ₅₀ | 8.5 | 7.5 | 3 |
| B ₇₀ | 7 | 6 | 2 |

Table. 2 Fitted anisotropy fields H_A , H_X , and H_U of B₁₀-B₇₀.

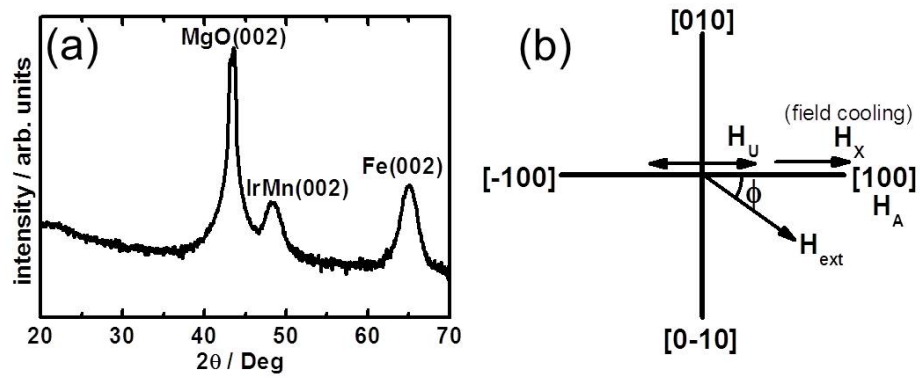


Fig. 1 (a) XRD θ - 2θ scan of Fe(10nm)/IrMn(8nm) EB bilayer. (b) Geometry of the field cooling direction, magnetic anisotropies and the external magnetic field.

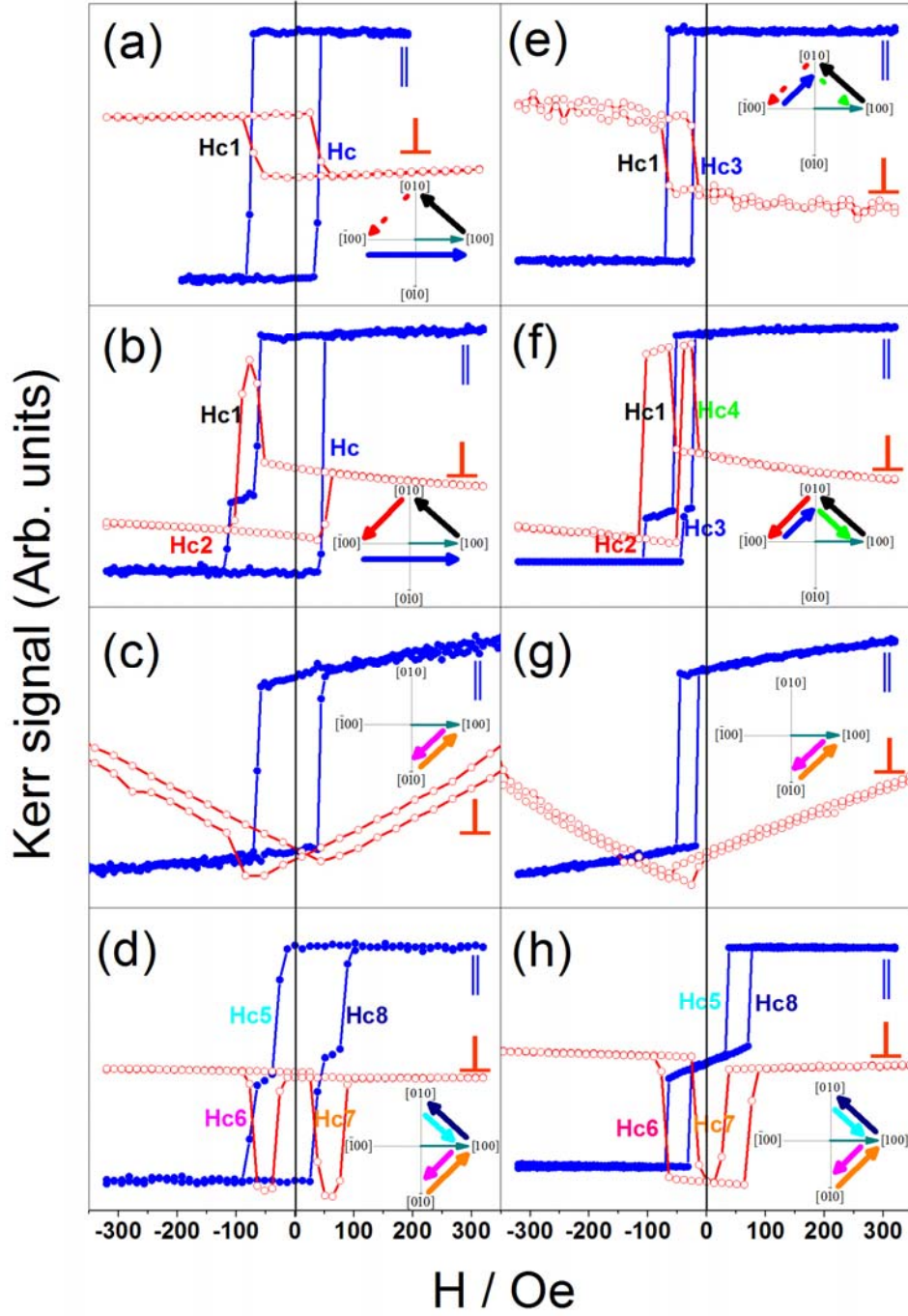


Fig. 2 (color online) Longitudinal (\parallel) and transverse (\perp) MOKE loops measured at various field orientations at $\phi=2.5^\circ$, $\phi=22.5^\circ$, $\phi=-42.5^\circ$, and $\phi=-87.5^\circ$ for A_{10} (a-d) and B_{10} (e-h). Inset figures illustrate the magnetization reversal process corresponding to the hysteresis loop. The switching fields in each main figure are shown by the arrows with corresponding colors in the inset figure. Dashed arrow indicates the

switching field that is not displayed during the two successive magnetic transitions.

The asymmetry (hysteresis) in transverse (\perp) signals in (a) and (b), at $\phi=2.5^\circ$, is due to the slight misalignment between MOKE laser beam plane and the magnetic field.

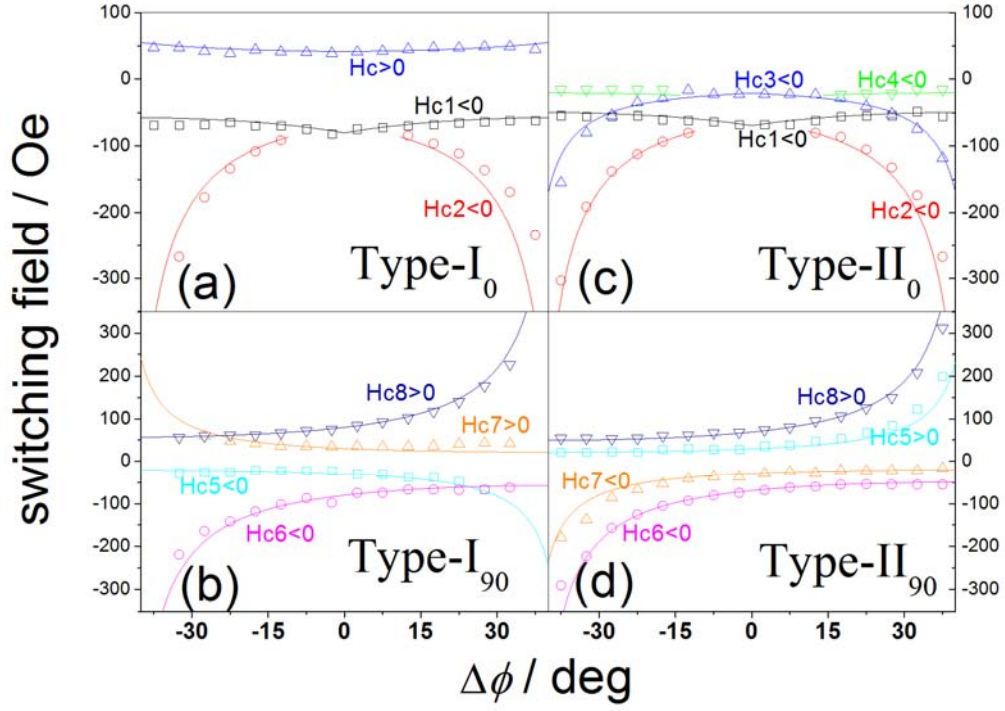


Fig. 3 (color online) Field orientation dependence of the experimentally observed switching fields (symbols) and the corresponding theoretical fittings (curves) for A_{10} and B_{10} . A_{10} exhibits the type-I₀ (a), and type-I₉₀ (b) angular dependent behaviors with the characterizing switching fields $H_{c1}<0$, $H_{c2}<0$, $H_c>0$ at ϕ_{\parallel} , and $H_{c5}<0$, $H_{c6}<0$, $H_{c7}>0$, $H_{c8}>0$ at ϕ_{\perp} . B_{10} exhibits the type-II₀ (c), and type-II₉₀ (d) angular dependent behaviors with the characterizing switching fields $H_{c1}<0$, $H_{c2}<0$, $H_{c3}<0$, $H_{c4}<0$ at ϕ_{\parallel} , and $H_{c5}>0$, $H_{c6}<0$, $H_{c7}<0$, $H_{c8}>0$ at ϕ_{\perp} .

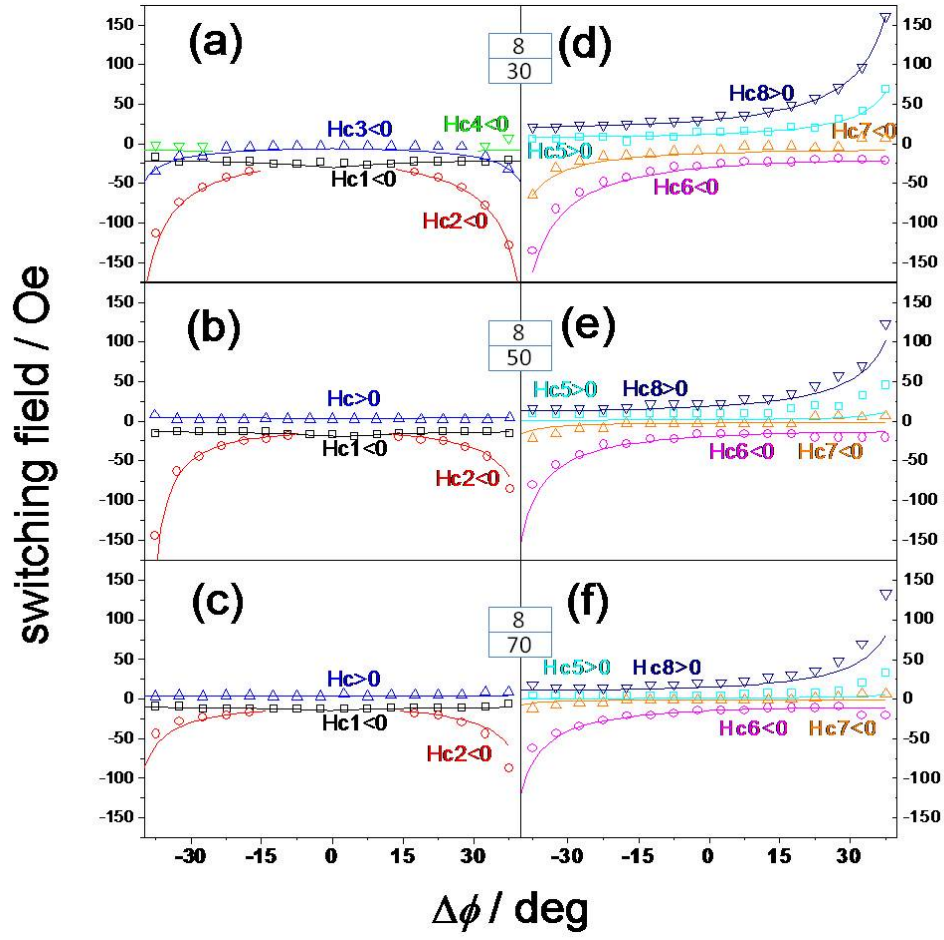


Fig. 4 (color online) Field orientation dependence of switching fields (symbols) and the corresponding theoretical fittings (curves) for B_{30} , B_{50} , and B_{70} at ϕ_{\parallel} (a,b,c), and at ϕ_{\perp} (d,e,f), respectively. Transition from type-II₀ (B_{30}) to type-I₀ (B_{50} , B_{70}) was verified at ϕ_{\parallel} ; however, no corresponding transition was observed at ϕ_{\perp} .

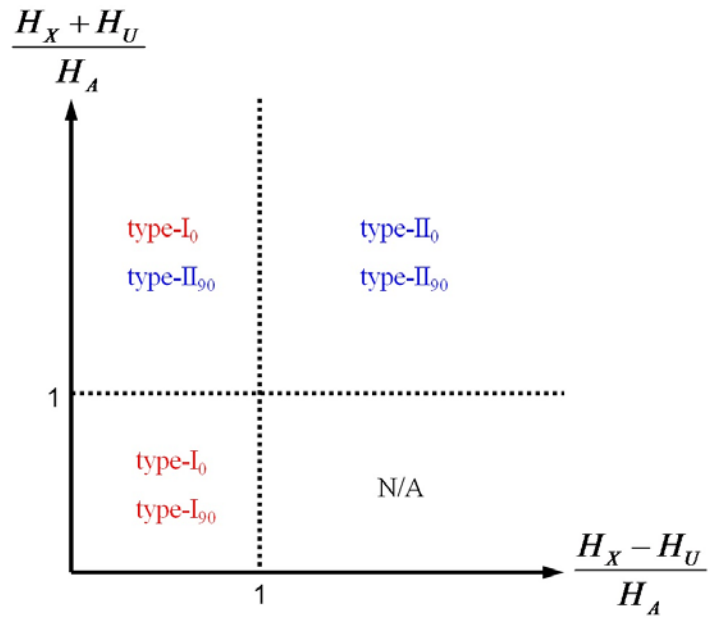


Fig. 5 (color online) Phase diagram showing the relationship between different types of angular dependent behaviors with the relative magnitudes of the effective anisotropy fields.